The International Journal of Advanced Manufacturing Technology (2022) 123:1521–1541
https://doi.org/10.1007/s00170-022-10254-8

ORIGINAL ARTICLE

Machining characteristics of various powder-based additives, dielectrics, and electrodes during EDM of micro-impressions: a comparative study

Kashif Ishfaq[1] · Muhammad Asad Maqsood[1] · Muhammad Arif Mahmood[2]

Received: 21 June 2022 / Accepted: 3 October 2022 / Published online: 14 October 2022
© The Author(s) 2022

Abstract
Electric discharge machining (EDM) has great acceptance in different application sectors to wipe out intrinsic problems, like product miniaturizing and tight tolerances, during the fabrication of micro-size products. Many researchers have worked well in the micro-cutting of various alloys through the EDM process. However, limited work has been reported on the EDM of SS 316 for micro-impression fabrication using EDM. The selection of the best dielectric, electrode material, and powder-based additives has never been targeted so far to have dimensionally accurate micro-impression at an appreciable cutting rate with no/less electrode damage in the EDM of the said alloy. Therefore, in this research, the collective influence of various dielectrics (kerosene oil, transformer oil, and canola oil), powders (alumina, graphite, and silicon carbide), and electrodes (copper, brass, and aluminum) have been comprehensively examined for the fabrication of micro-impressions in AISI 316 using EDM. Taguchi L9 orthogonal technique was applied to study the effect of four input parameters on material removal rate, overcut, and tool wear rate. Results were statistically explored using main effect plots and supplemented by scanning electron microscopy, surface profilometry, and optical microscopy. The results show that material removal and tool wear rates notably improved from the mean value by 29% and 89.4%, respectively, when the machining is carried out under silicon carbide mixed kerosene dielectric against silicon carbide the aluminum tool at a pulse time ratio of 1.5. Furthermore, for dimensional overcut, 5.3 times lesser value is observed from the average magnitude of 0.189 mm when the proposed EDM setup is employed for cutting AISI 316. An optimized setting has also been proposed by grey relational analysis and then validated through a confirmation experiment.

Keywords EDM · AISI 316 · Additives · Dielectrics · Electrodes · Micro-impression

1 Introduction

Currently, the demand for micro-products is rapidly increasing due to advancements in tools and technologies. Micro-products/components have wide importance in biotechnology, optics, electronic items, automobiles, and avionics industries [1]. However, organizations still have some challenges, i.e., product miniaturization and industrial awareness of micro-engineering. To set the limitations aside, micro-machining has been proved a critical technology [2].

Different physicochemical processes can be used for micro-machining, including milling, turning, drilling, electrochemical machining, energy beam machining, and electric discharge machining (EDM) [3]. Amongst these, conventional technologies have dropped in popularity because of material removal rate (MRR) issues, poor dimensional control, and high tool wear rate (TWR) [4]. In such mechanical processes, the tool is also damaged due to the direct connection with the workpiece, resulting in high residual stress, which can alter the micro-features on the machined cavity [5, 6]. To overcome the barriers mentioned above in traditional technologies, researchers have attempted non-conventional means especially micro-electric discharge machining (μ-EDM), predominantly for those applications where MRR, TWR, and dimensional overcut (OC) are primary concerns

✉ Muhammad Arif Mahmood
muhammad.arif_mahmood@outlook.com

[1] Department of Industrial and Manufacturing Engineering, University of Engineering and Technology Lahore, Lahore 548900, Pakistan

[2] Mechanical Engineering Program, Texas A&M University at Qatar, PO Box 23874, Doha, Qatar

[7–9]. Among the various derivatives of non-conventional processes, μ-EDM has been employed in this investigation owing to its numerous advantages like cost-effectiveness and ability to produce complex/intricate geometries with tight tolerances. [10, 11].

Micro-EDM is a stochastic process and works on the material removal principle [12]. In this process, an electrically conductive material is placed in a dielectric fluid (usually kerosene oil). A precisely controlled series of discrete electric sparks are generated in the workpiece-electrode gap, raising the cutting zone temperature to 12,000 °C [13]. Subsequently, a small amount of material is chipped off in the melted debris from the electrode and workpiece [14]. The removed debris/chips are flushed away by the dielectric. Some of the debris again re-solidified and cooled down over the machined surface due to the presence of dielectric fluid [15–17]. A number of responses have been considered by researchers in the literature, while EDM of stainless steel (SS), due to their prominence in micro-machining [18–21]. Such as, the noticeable value of material removal rate (MRR) is principally needed to justify the machining cost, whereas tool wear rate (TWR) accounts for waste reduction, which is a fundamental requirement of sustainable machining. However, dimensional accuracy or overcut (OC) is a prerequisite for the accurate functionality of the finished product [22]. Considering the significance of the responses related to the cutting of different alloys, especially SS AISI 316, all three responses (MRR, TWR, and OC) have been chosen as output parameters for this investigation.

Since the values of machined inputs significantly affect the responses, i.e., MRR, TWR, and OC, selecting input parameters is equally important along with outputs [23]. Different studies were reported on cutting SS AISI 316 material using various EDM parameters to evaluate the machining performance. For instance, Ramachandra [24] measured MRR and surface roughness (SR) during EDM of AISI 316 employing response surface methodology (RSM). Duty cycle, on-time (T_{on}), and discharge current (DC) were taken as control variables, whereas electrode material was copper. The results concluded that DC was the most influential factor while measuring SR and MRR. Another researcher [25] optimized the process parameter during EDM of AISI 316 LN SS using the concept of fuzzy logic and particle swarm optimization (PSO). Pulse current, T_{on}, and off-time (T_{off}) were the input factors, whereas MRR and electrode wear rate (EWR) were the output responses. A single optimized parametric setting was proposed and validated. Considering the same input parameters, Makwana and Banker [26] studied the effect of alternation in tool (pure copper) profile on the EDM performance of AISI 316 SS using Taguchi's design. They summarized that circular tool geometry was optimal because it delivered a smooth finish followed by triangular and rectangular shapes. It was also reported that an increase in current amplified MRR, TWR, and SR values. They also claimed to have a thinner heat-affected zone, micro-cracks, and a thicker recast layer at higher current and T_{on} values.

Safiei et al. [27] performed EDM of SS 316L using a copper electrode impregnated with graphite. MRR, TWR, SR, and OC were evaluated against peak current (I_p), servo voltage, T_{on}, and T_{off}. They said servo voltage was an insignificant factor, whereas I_p has a noticeable impact on the defined responses. They suggested optimal parametric settings for achieving minimum TWR, SR, OC, and maximum MRR, such as I_p (40.9 amperes), T_{on} (80 μsec), and T_{off} (60 μsec). Ahmed et al. [28] explored micro-impressions on a biomedical material, namely Ti-6Al-4V, employing EDM process. They investigated dimensional errors, SR, and tool length reduction (TLR) against three input factors: pulse time ratio (PTR), DC, electrode material, and tool polarity. They claimed that Cu-electrode with negative polarity is the best combination for EDM of Ti-6Al-4V, meeting the need of all four responses. The surface textures obtained were good for Al-electrode, with an SR of 1.05 μm. This value of SR was approximately eight times less than the value attained with the graphite electrode. Ishfaq et al. [29] investigated geometrical errors (axial and lateral overcut) in EDM of AISI D2 steel for dies and mold repairing applications. It was revealed that the mean value of lateral errors is 2.5 times higher than axial errors. However, the copper electrode is an appropriate choice to reduce axial errors, followed by tungsten carbide and graphite. Chen et al. [30] probed the effect of various electrode materials (brass, tungsten, and copper tungsten) during powder mixed EDM (PMEDM) of Ti-6Al-4V. The copper tungsten electrode was best rated to machine the aforesaid Ti-alloy because it has a high throughput rate (75.2%), a thinner RLT (3.35 μm), a small TEW (139 μm), and a high MRR (255.39 mm^3/min).

Wang et al. [31] studied the machining characteristics of EDM of Ti-alloy using nanographene in the context of MRR, SR, and relative electrode wear (REW). It was cited that MRR improved by 28%, whereas the value of SR and REW dropped by 55% and 43%, respectively, if graphene was used. Pour et al. [32] noticed the effect of ZnO nanoparticles and peak current on the EDM of various cutting materials, including AISI 1045, AISI 4140, and AISI D3. They reported that MRR notably increased up to 45.55%, 33.33%, and 10.71% during rough cutting of AISI D3, AISI 4140, and AISI 1045, respectively if peak current was set at 18 A using 4 g ZnO. However, for SR, improvements were seen up to 16.66%, 29.41%, and 56.25% for AISI 1045, AISI 4140, and AISI D3, respectively. Tiwary et al. [33] explored the impact of different dielectrics (EDM oil, deionized water, and Cu-powder mixed deionized water) on the micro-EDM of Ti-6Al-4V. They summarized that all the responses above are improved when copper powder mixed with deionized water is utilized instead of other dielectrics.

The literature review shows that limited work has been reported on the EDM of SS 316 for micro-impression fabrication using EDM. The selection of the best dielectric, electrode material, and powder-based additives has never been targeted so far to have dimensionally accurate micro-impression at an appreciable cutting rate with no/less electrode damage in the EDM of the said alloy. Therefore, in this research, the collective influence of various dielectrics (kerosene oil, transformer oil, and canola oil), powders (alumina, graphite, and silicon carbide), and electrodes (copper, brass, and aluminium) have been comprehensively examined for the fabrication of micro-impressions in AISI 316 using EDM. In the published work, the evaluation of MRR, TWR, and OC is not broadly explored yet during EDM of said alloy to analyze the micro-texture of the machined cavities against the combined influence of aforenamed factors. Thereof, the main focus of this research is to evaluate the MRR, TWR, and OC against the four input parameters, i.e., dielectric type, powder type, electrode type, and PTR, as far as μ-EDM of AISI 316 is taken into account. Taguchi's DOE has been selected for machining. The outcomes of all nominated responses are statistically examined against the set of input parameters. The results have been supplemented by optical microscopy, scanning electron microscopy (SEM), and surface profilometry for detailed insight into the findings. The optimal setting was proposed using gray relational analysis (GRA) and confirmed against the defined responses.

2 Material and methods

In this investigation, AISI 316 has been utilized as a workpart material due to its common use in biomedical applications such as orthopedic implants, cardiovascular stents, and dental implants. Besides biomedical sectors, the selected workpiece is also applied in many engineering, chemical, petrochemical, and marine industries [34]. The tremendous popularity of AISI 316 is due to its salient properties, including high corrosion resistance, great strength, and excellent creep resistance [35]. The experimental setup was arranged on die sinking EDM (Model: CJ-230 Creator, Taiwan). The schematic and fundamental principle of EDM is displayed in Fig. 1. Three circular cross-sectional electrodes (Al, brass, and Cu) were engaged during the machining of the material mentioned above, as shown in Fig. 2. Each electrode has a diameter of 12 mm. In addition to that, three different dielectrics (kerosene oil, transformer oil, and canola oil) and powders (aluminium oxide (Al_2O_3), graphite, and silicon carbide (SiC)) were also practiced. The selection of the different types of dielectrics, powders, and types of electrode materials has been made on a particular rationale. The dielectrics, powders, and electrodes engaged in the study have already proved their potential in EDM of various materials. These electrodes, powders, and dielectrics were common in practice as per the available literature [36–42]. However, their potential has never been targeted for the fabrication of micro-impressions in SS316. But the appropriate selection

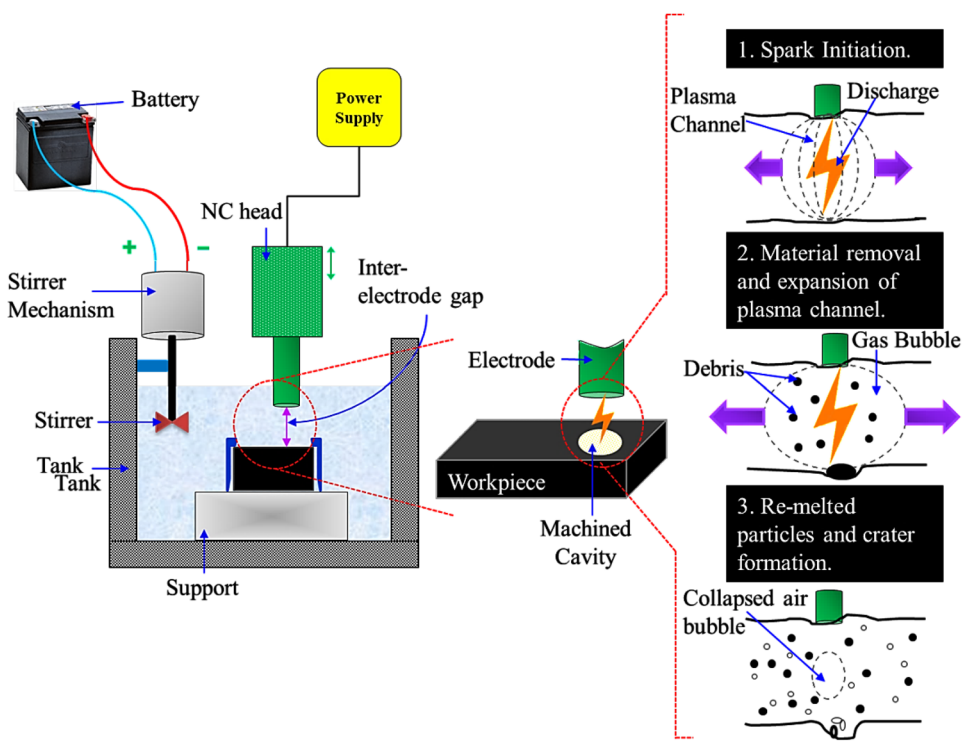

Fig. 1 Schematic and basic principle of EDM die sinker

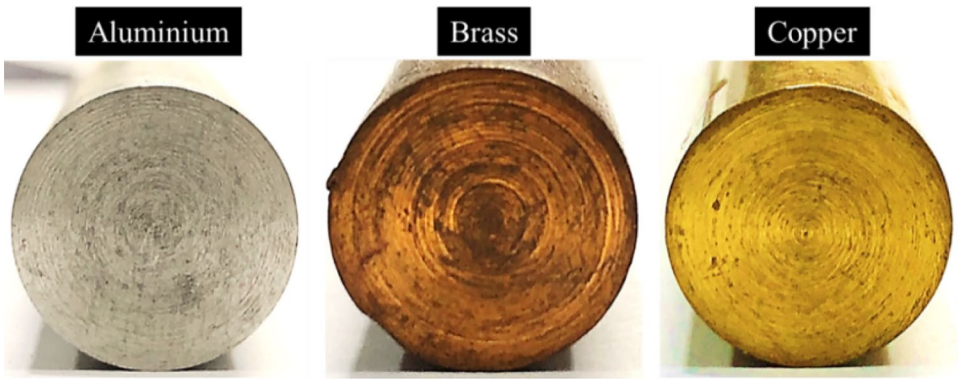

Fig. 2 Electrode materials

of the said control variables is an essential requirement to have a substantial cut quality of the micro-machined impression. The criticality of selecting the aforementioned control parameters further signifies that the micro-machined impression with tight tolerance and a good cutting rate is the desired outcome. For that reason, the current study employed the abovementioned electrodes, powders, and dielectrics during EDM of AISI 316 to propose the best combination of control variables. The prime characteristics of the mentioned dielectrics are tabulated in Table 1.

The literature database was consulted for initial guidance of parametric levels' settings. However, afterward, preliminary trials were performed. Based on those trials' findings, input variables' levels were defined. Those level values were selected to ensure uniform sparking for producing a complete machined impression on the work. Another aspect in EDM, i.e., arcing, was given due consideration during level selection. It has been confirmed that only those parametric levels should be engaged in the EDM, which minimizes the chance of arcing. The details about input factors' levels used for actual experimentation have been tabulated in Table 2.

The present study analyzed the MRR (g/min), TWR (g/min), and OC (mm) against the set of four input parameters, i.e., dielectric type, powder type, electrode type, and PTR. The rate of material erosion, or MRR, is the amount of material eroded per unit of time. To compute it, the weight of the workpiece before and after the experiment was recorded along with the time taken for the experimental cut. Equation (1) was applied to calculate the MRR of the machined cuts.

$$\mathrm{MRR} = (W_B - W_A)/T \tag{1}$$

where W_B is the weight of the workpiece before the cut, W_A is the weight of the workpiece after the cut, and T is the time of cut.

The electric sparks in the EDM process cause the material to erode from the workpiece and electrode. As a result, the dimensional accuracy of the machined profile got affected. It makes the TWR an essential factor to be considered while machining. The tool wear rate can be estimated by the weight difference of the tool before and after the experiments, represented in Eq. (2).

$$\mathrm{TWR} = (W_{BT} - W_{AT})/T \tag{2}$$

Here, W_{BT} (g) is the tool weight before cut; W_{AT} (g) is the tool weight after the cut. The third response, namely OC, was equally essential in machining because it decides the proper functionality of parts/products. The difference between the machined cavity's size and the tool's diameter is known as the OC. It is calculated by using Eq. (3).

$$\mathrm{OC} = (\mathrm{DC} - \mathrm{DT}) \tag{3}$$

Here, DC is the diameter of the machined cavity, and DT is the tool diameter in millimeters (mm). The selection of aforesaid input parameters was based on the given

Table 1 Some features of dielectrics

Serial no.	Properties (units)	Kerosene oil	Canola oil	Transformer oil
1	Visual	Clear	Clear	Clear
2	Specific gravity (g/ml)	0.82	> 1	0.84
4	Flash point (K)	311.15	603–633	413.15
6	Pour point (K)	243.15	253.15	243.15
5	Dielectric strength (kV)	14.3	33	57
7	Moisture content (ppm)	125.3	833	51.3

Table 2 Parametric levels and constant variables

Input factors	Input variables			Constant variables	
	1st level	2nd level	3rd level	Parameters (units)	Values
Dielectric type	Kerosene oil	Transformer oil	Canola oil	Depth of cut (mm)	0.5
Electrode material	Copper	Brass	Aluminium	Pulse off time (μs)	50
Powder type	Alumina	Graphite	Silicon carbide	Dielectric quantity (ml)	250
Pulse time ratio	0.5	1.0	1.5	Discharge current (A)	15
				Powders' concentration (g/l)	1.0

considerations. (1) Input factors have a great impact on responses, (2) or the influence of particular parameters is not previously studied on the responses [22]. The rest of the factors, other than the above, were set as constant, as mentioned in Table 2. To find parametric levels, preliminary trials were performed before actual experimentation. The defined levels of each parameter are also compiled in Table 2. A separate container was designed and fabricated, with a half-liter storage capacity of the dielectric. It consists of a stirrer mechanism (see Fig. 1) to make a homogenous mixture when 1 g/l powder is added to the 250 ml dielectric. Taguchi's L9 orthogonal array was used to carry out experiments. A computerized numerical control (CNC) coordinate measuring machine (Model: CE 450 DV) was employed to measure diametric overcut.

Statistical testing thoroughly investigated the results, i.e., main effect plots, for examining the responses against input parameters. Evidence was gathered through an optical microscope and SEM analyses. Additionally, 3D surface plots were also collected with the aid of surface profilometry. After a comprehensive discussion, an optimal combination against each response was suggested. Finally, the GRA method has suggested the optimal setting and validated it by performing confirmation experiments. The facets involved in the GRA approach are described in the imminent section.

GRA is a multiobjective optimization technique for correlating input parameters and output responses. It is a highly user-interactive and multifaceted problem-resolving approach. The steps include in this technique are enlisted in Fig. 3.

In the very initial step (gray relational (GR) generating), all the possible alternatives have been altered into comparability order by assigning a scale from 0 to 1. Based on narrated relations, the results of the given responses are examined. For instance, in the present study, MRR, TWR, and OC have been inspected against the four parameters. Thus, a higher value of MRR and a smaller value of TWR and OC are acceptable. Thus, the criteria "larger is better" and "smaller is better" were computed by using Eqs. (4) and (5), respectively.

$$X_i(k) = \frac{Y_i(k) - minY_i(k)}{maxY_i(k) - minY_i(k)} \tag{4}$$

$$X_i(k) = \frac{maxY_i(k) - Y_i(k)}{maxY_i(k) - minY_i(k)} \tag{5}$$

where $X_i(k)$ = normalized value, $Y_i(k)$ = value in the column for response k, $\min Y_i(k)$ = smallest value in the column for response k, $\max Y_i(k)$ = largest value in the column for response k.

Fig. 3 Steps of GRA

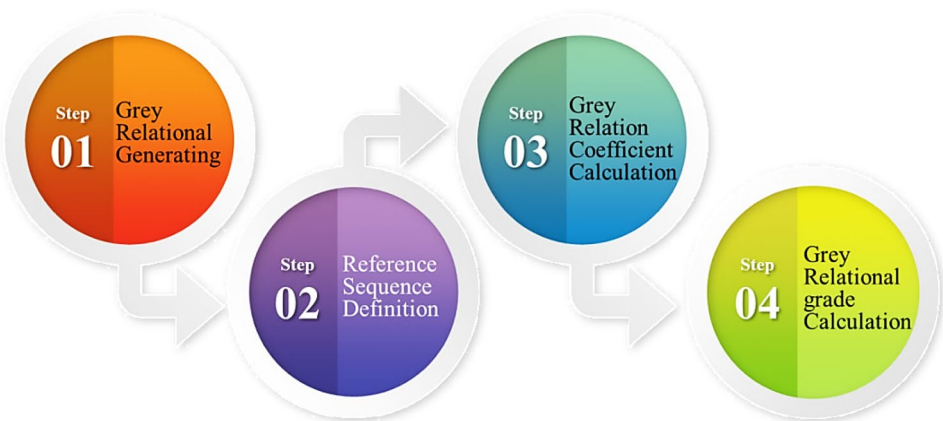

In the second stage (reference order/sequence definition), the novel alternative is selected by computing the performance magnitude whose answer is nearly equal to 1. Afterward, the definition sequence is calculated by relating it with the reference order.

The GR coefficient (GRC) is enumerated in the third step using Eq. (6).

$$\gamma_i = \frac{\Delta_{\min} + \zeta\Delta_{\max}}{\Delta_{\mathrm{oi}}(\mathrm{k}) + \zeta\Delta_{\max}} \tag{6}$$

Here, γ_i= GRC for an ith experiment of the response k, ζ= differentiating coefficient (its value ranges from 0 to 1), $\Delta_{\mathrm{oi}}(k)$ = difference between absolute value, $\Delta_{\min}$ = minimum value of $Y_i(k)$, and $\Delta_{\max}$ = maximum value of $Y_i(k)$. To compute Δ_{oi}, Eq. (7) is developed.

$$\Delta_{oi} = \left|X_o(k), -X_i(k)\right| \tag{7}$$

In the last phase, GR grade (α) is computed using Eq. (8). It evaluates the experimental outcomes of the multiresponse characteristic. The highest value of the GR grade depicts the optimal level of experiments.

$$\alpha = \frac{1}{\mathrm{n}}\sum_{k=1}^{n} \mathrm{Y_i(k)} \tag{8}$$

where n indicates the number of responses.

3 Results and discussion

This section covers a comprehensive discussion of the effect of various selected parameters on the MRR, TWR, and OC. For that purpose, main effect plots were drawn through Minitab software. Each response was separately discussed against a set of parameters, as demonstrated in the forthcoming section. The outcomes of each output and a DOE are provided in Table 3.

3.1 Material removal rate versus input parameters

The main effect plot presented in Fig. 4 shows the influence of chosen parameters on the MRR. According to Fig. 4, MRR is evaluated against every three parameter levels. In the case of dielectric type, three oil, namely kerosene, transformer, and canola, were utilized to analyze the rate of material erosion while machining AISI 316 on EDM. It has been noticed that maximum MRR was achieved with the transformer oil compared to the rest of the dielectrics. High dielectric strength, high flash point, and resistance to thermal oxidation are the main reasons transformer oil eroded more material from the workpiece. Because of the above characteristics, a spark under transformer oil is quickly generated, resulting in high MRR [43]. However, the material removal rate is highly diminished when canola dielectric is considered more than kerosene oil due to low dielectric strength and viscosity. Hence, transformer oil is ideal compared to kerosene and canola dielectrics, which deliver maximum MRR as far as EDM of AISI 316 is concerned. The surface texture obtained under each dielectric is presented in Fig. 5. According to Fig. 5, it can be noticed that the surface obtained under kerosene and transformer oils contains more redeposited particles as compared with canola oil. A large number of craters is found on the surface of the workpiece when the two hydrocarbon-based dielectrics are employed. On the other side, the surface texture achieved with canola is the finest, followed by the rest of the cases. This happened due to the intrinsic properties of canola oil, such as high flash point, high fire point, large viscosity, and excellent biodegradability.

The effect of three electrodes (Cu, brass, and Al) on MRR is also noticed herein, as depicted in Fig. 4. An opposite

Table 3 Evaluation of output factors versus input parameters

Sr.	Input parameters				Output factors		
	Dielectric type	Electrode type	Powder type	Pulse time ratio	MRR (g/min)	TWR (g/min)	OC (mm)
1	Kerosene oil	Copper	Al_2O_3	0.5	0.072	0.017	0.35
2	Kerosene oil	Brass	Graphite	1.0	0.039	0.047	0.11
3	Kerosene oil	Aluminum	SiC	1.5	0.111	0.019	0.03
4	Transformer oil	Copper	Graphite	1.5	0.144	0.022	0.45
5	Transformer oil	Brass	SiC	0.5	0.051	0.074	0.03
6	Transformer oil	Aluminum	Al_2O_3	1.0	0.142	0.030	0.08
7	Canola oil	Copper	SiC	1.0	0.122	0.019	0.45
8	Canola oil	Brass	Al_2O_3	1.5	0.047	0.058	0.11
9	Canola oil	Aluminum	Graphite	0.5	0.043	0.037	0.09

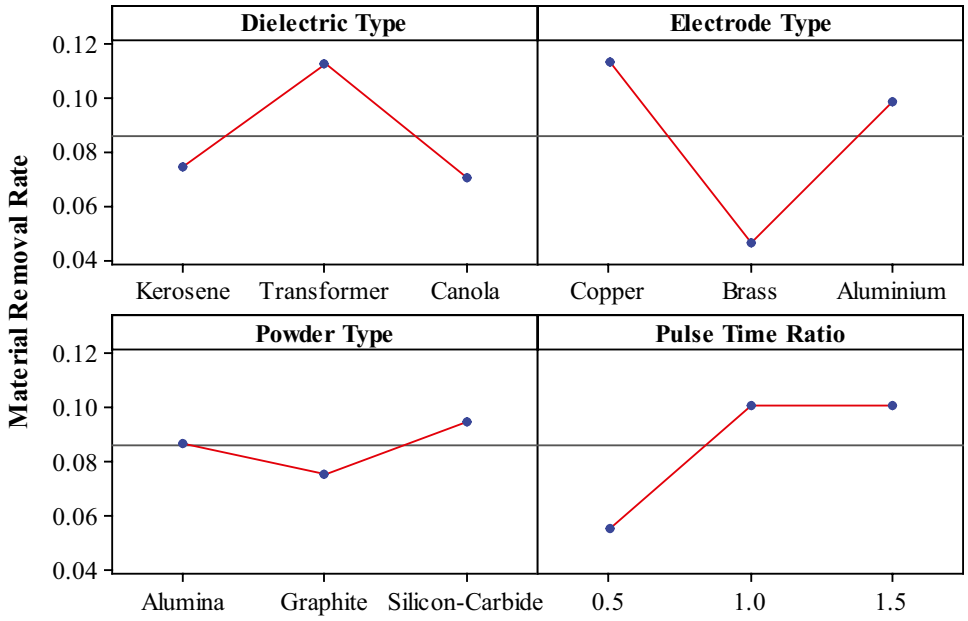

Fig. 4 Parametric plot representing the effect on MRR versus each input parameter

trend is observed from copper to aluminum electrodes when a comparison has been made with the trend of dielectric types. A copper electrode is outperformed in terms of MRR among all the selected electrodes because of its high (398.0 W/mK) thermal conductivity, followed by aluminum (227.0 W/mK) and brass (109.0 W/mK). It indicates that more heat is conducted through the copper electrode, generating high-intensity spark energy in the work-electrode space. The extraordinarily high strength of discharge energy attacks the cavity of the workpiece. It leaves large and deep size craters, as presented in Fig. 6a, then other craters formed by brass and aluminium electrodes, as shown in Fig. 6b, c. Subsequently, MRR is increased. Due to low thermal conductivity, lower melting point, and high electric resistance value, MRR is notably improved with the brass electrode [44]. However, MRR again upsurges with the aluminium electrode but is still not considered favorable compared to other tool materials. The comparison between different sizes of craters on the machined cavity by selected electrodes is depicted in Fig. 6. While the 3D surface profilometry against the copper electrode is also collected and portrayed in Fig. 7. Therefore, the copper electrode is suggested to get maximum MRR while cutting AISI 316 material through the EDM process.

In the dielectric medium, different powders, i.e., alumina, graphite, and silicone-carbide, are also discussed to examine the MRR, as shown in Fig. 4. Amongst these powders, the powder of SiC has provided superb results of MRR during EDM of AISI 316, irrespective of considering the other parameters. One of the published works said that the addition of SiC powder magnifies the conductivity, lowers the breakdown strength of the dielectric liquid, and increases the discharge gap, which enhances the MRR by several folds [45, 46]. The surface morphology of the machined cavity under SiC powder is displayed in Fig. 8a. In the same analogy, alumina is the second-best powder for

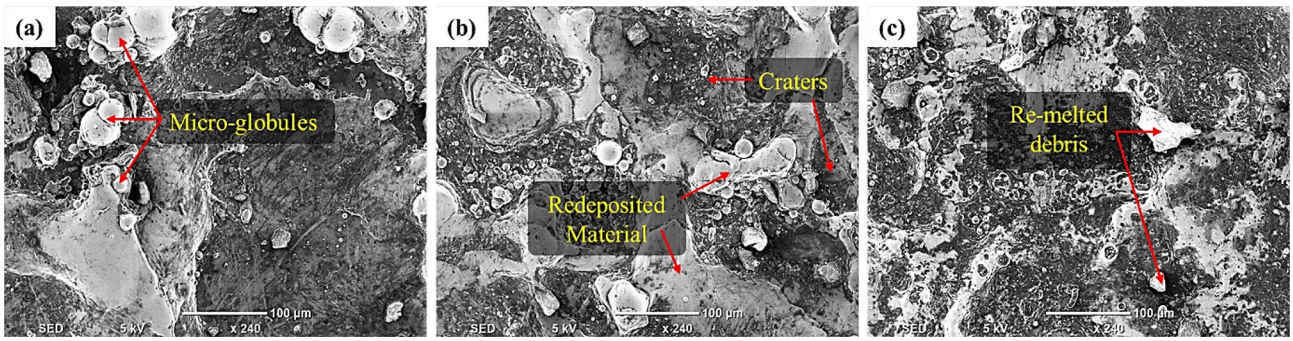

Fig. 5 Surface texture obtained under various dielectrics: **a** transformer oil, **b** kerosene oil, **c** canola oil

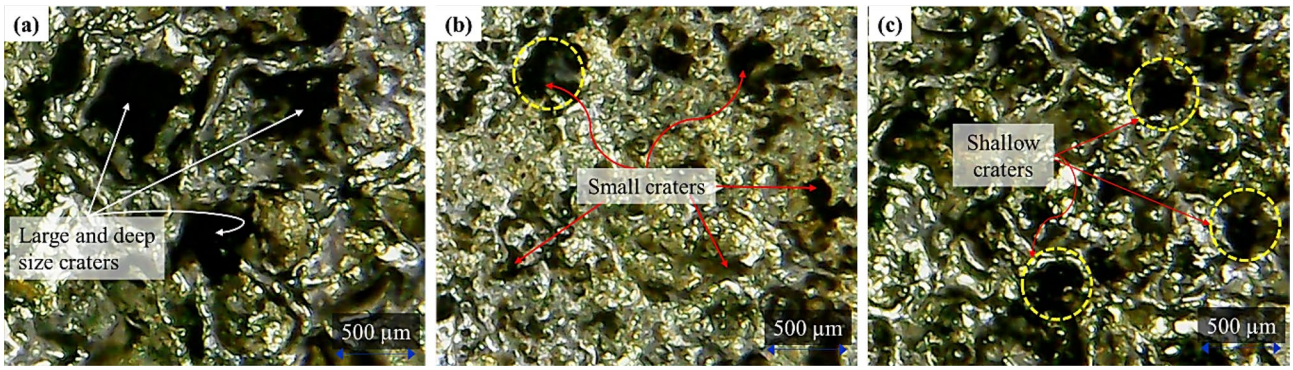

Fig. 6 Micrographs show the different sizes of craters on the workpiece's surface against different electrodes: **a** copper, **b** brass, and **c** aluminum

getting a high value of MRR. Interestingly, MRR is significantly lowered when graphite powder is added to the dielectric liquid; however, its thermal conductivity (704 W/mK) is much higher than other powders. The low magnitude of MRR under graphite powder is due to its accumulation in the machining zone, resulting in a protective layer above the surface that prevents the removal of particles from the workpiece. Eventually, MRR is reduced [47]. SEM images provided in Fig. 8b, c show the surface texture attained under alumina and graphite powders, respectively. It is interesting to note that the volume of redeposited melt is greater in the case of SiC powder, followed by graphite and alumina, as shown in Fig. 8. It is attributed to the high thermal conductivity of SiC powder (490 W/mK) compared to other powders (alumina = 35 W/mK and graphite = 1.50 W/mK). The effect of high thermal conductivity influences the material resolidification rate; it becomes faster. As a result, removed material gets redeposited over the workpiece's surface [48]. Moreover, many small size craters are observed over the machined profile in the case of alumina powder. Dispersion of discharges governed by the large inter-electrode gap is the key reason behind the topology achieved with alumina powder. At the same time, the lower thermal conductivity of graphite powder permits greater heat flux into an electrode and lowers the heat dissipation rate [49]. This tends to produce shallow craters with redeposited melt on the machined cavity, as witnessed in Fig. 8c. In a nutshell, EDM of AISI 316 is highly appreciable under silicone-carbide powder, given attaining high MRR.

Pulse time ratio (a ratio between pulse on-time and pulse off-time) is also studied against MRR at three defined levels during cutting AISI 316 through the EDM process. The trend of PTR is portrayed in Fig. 4. It has been seen that PTR is linearly proportional to the MRR from level 1 (0.5) to level 2 (1.0). As pulse-off time is constant, say 50 µs, PTR is only proportional to the pulse-on time. It is observed that an increase in T_{on} up to 50 µs also upsurges the MRR due to an increase in the intensity of spark over the machined surface, which removes the material from the workpiece in both the cutting orientation (radial and

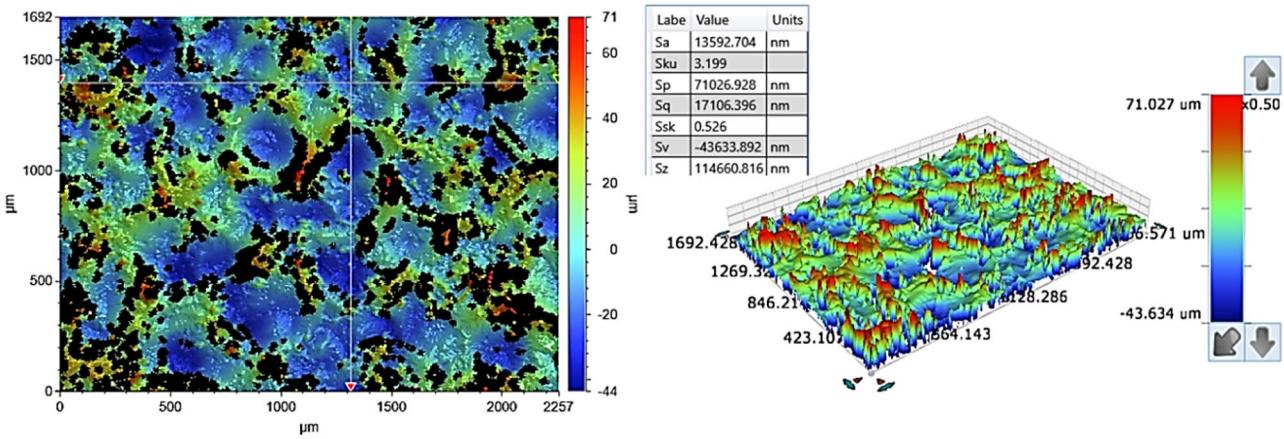

Fig. 7 3D surface profile when Cu-electrode is used for the EDM of AISI 316

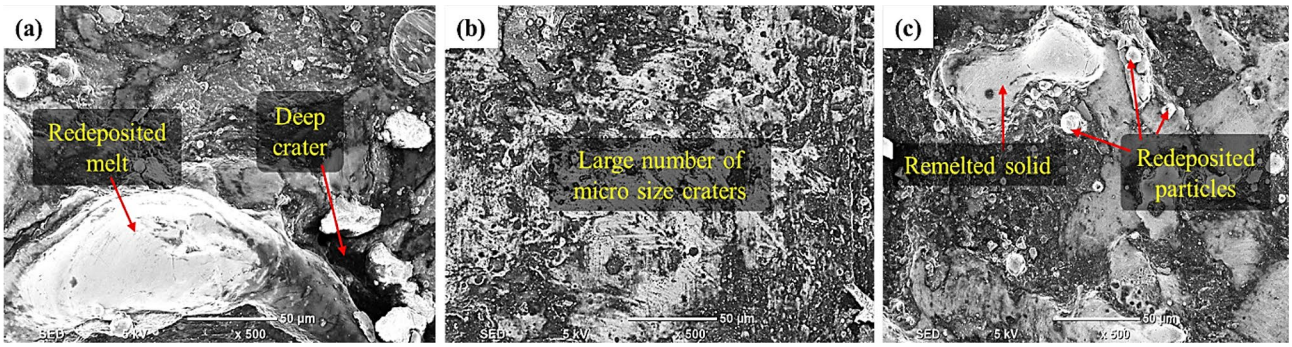

Fig. 8 Surface morphology of machined cuts under different powders such as **a** silicon carbide, **b** alumina, and **c** graphite

lateral), leading to high MRR by leaving deep craters on the surface [50]. With the further increase in PTR up to 1.5, MRR almost remains constant because of the excessive discharging rate at an extremely high value of T_{on} that further undergoes intensive ionization of the dielectric particles, which made a shield above the machined cavity, causing a little hindrance in front of discharging but due to high kinetic energy of ions yielded deep craters on the machined cut. Figure 9 demonstrates the different sizes of craters found on the work part's surface at all three PTR settings. Thus, the value of MRR does not affect substantially. Hence, levels 2 and 3 are the most permissible for machining AISI 316 with EDM.

Besides discussing the main effect plot of MRR, interaction plots have also been made to study the relationship between one factor and response to another factor, as shown in Fig. 10. It can be seen that each plot displays different interactions between four input parameters. For instance, all three dielectrics interact when the brass electrode is employed during EDM of AISI 316. Between powder type and dielectric type, interactions at two points are noticed. No relationship can be observed among the three dielectrics for alumina powder, as long as the said interaction is considered. But, for the same powder, transformer oil is the one that has yielded a significant value of MRR, followed by kerosene and canola oil. In the same way, when the relationship between dielectric type and pulse time ratio is deliberated, transformer oil only intersects at one point with the kerosene oil, while kerosene oil has two different interactions at level 1 (0.5) and level 3 (1.5) of PTR, as portrayed in Fig. 10. Furthermore, it is interesting to foresee that no interaction is perceived between SiC and various electrodes. However, for SiC powder, maximum MRR is attained with the copper electrode. When the relationships between PTR and electrode type are examined, brass is the only electrode that delivers single interaction with aluminium at the minimum value of PTR. Contrarily, the aluminium electrode provided different interactions with other electrodes at all three levels of PTR. In the last plot, the interaction between PTR and powder type is studied, in which relationships between different powders are found at a higher value of PTR.

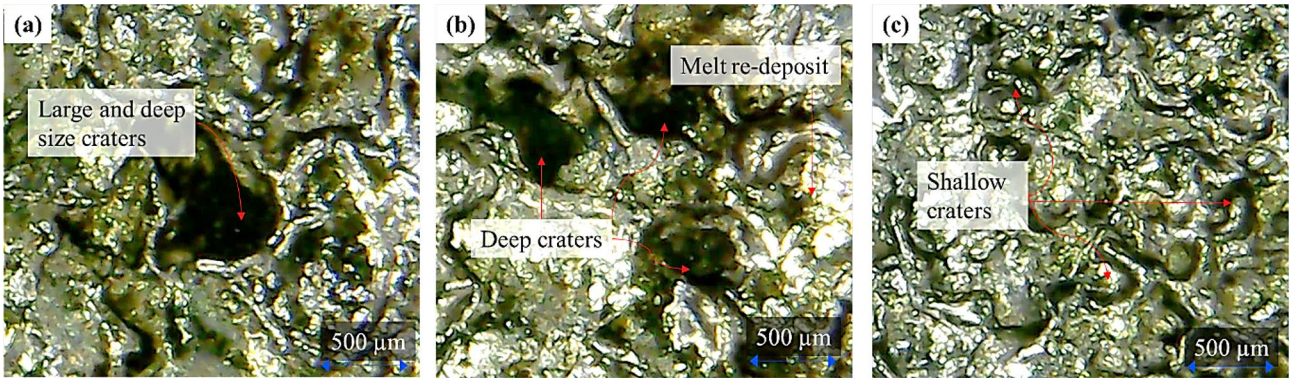

Fig. 9 Different sizes of craters formed on the specimen's surface at different levels of PTR, such as **a** 1.0, **b** 1.5, and **c** 0.5

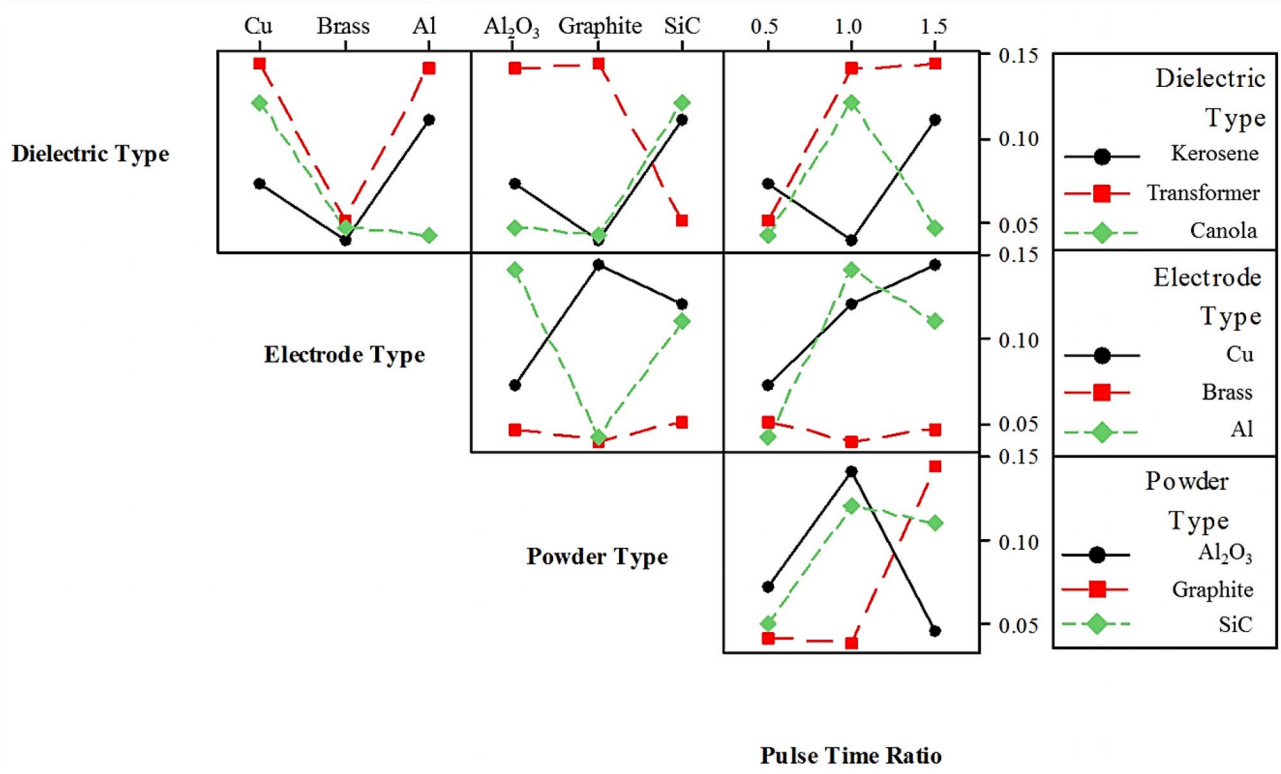

Fig. 10 Interaction plot (data mean) of material removal rate

3.2 Tool wear rate versus input parameters

Tool wear rate is another measurable factor that is evaluated in this study during the cutting of AISI 316 material by applying the EDM process. Similar to the MRR, this response is also examined at each selected parameter level. The main effect plot shown in Fig. 11 indicates how TWR varies with the change in parametric levels. For instance,

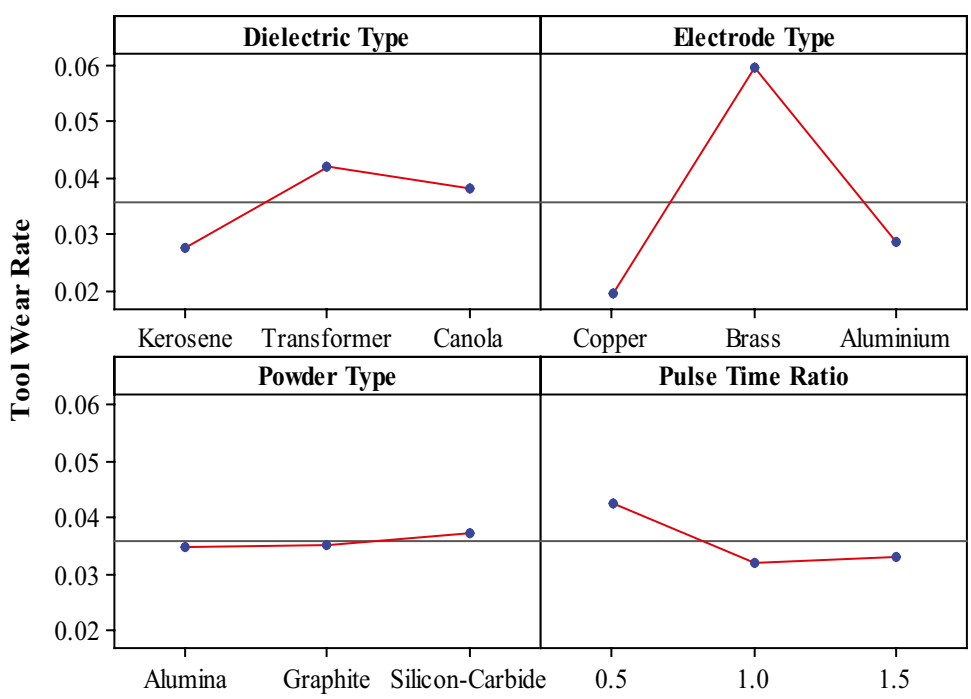

Fig. 11 Variation of TWR against four input parameters

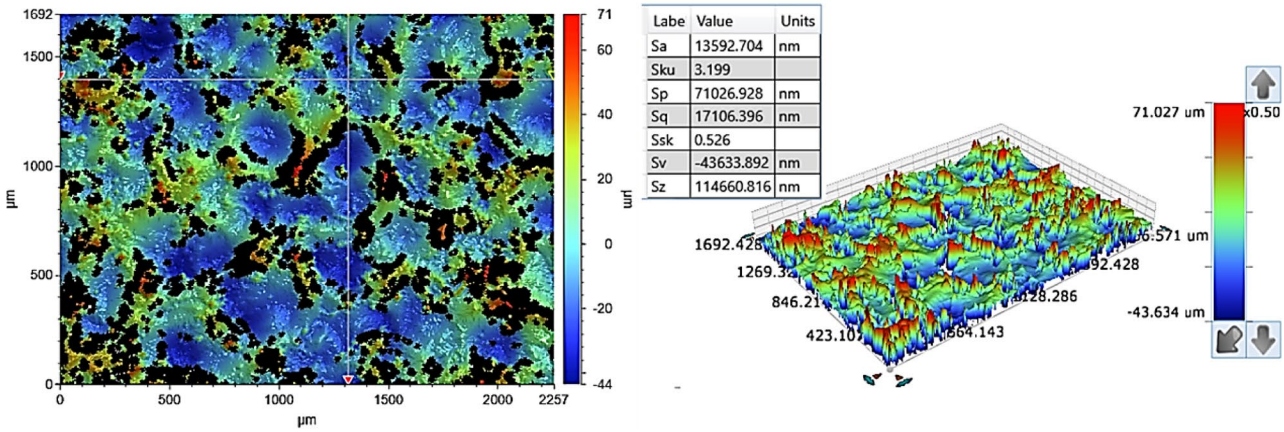

Fig. 12 3D surface profile of AISI 316 under kerosene dielectric fluid

kerosene oil has delivered superior results regarding TWR, followed by canola and transformer oil in the case of dielectric types. As per the literature, the dielectric's low viscosity and specific gravity are the two fundamental properties that improve the responses [50]. As kerosene has low viscosity (1.2199 cSt at 40 °C), followed by canola oil (5.8 cSt at 40 °C) and transformer oil (9.6 cSt at 40 °C); therefore, lower tool wear rate is observed with kerosene dielectric. In addition to that, low viscosity improves the cooling and flushing effect of the dielectric fluid, minimizing obstacles for heat transfer toward the work part. Thus, no heat is accumulated in the electrode, resulting in less TWR [51]. Contrarily, electrode wear rate is significantly compromised when transformer oil is used as dielectric during EDM of AISI 316. The high viscosity of transformer oil is the primary reason behind the high TWR.

Contrary to the above, high viscosity causes process instability because of inappropriate flushing. As a result, less energy is transferred to the work part, and major heat energy is accumulated around the electrode's periphery. Due to the high intensity of heat, TWR is raised. It has also been seen that canola oil performs better than transformer oil in TWR but is not as good as kerosene due to low breakdown voltages and high oxygen content than hydrocarbon-based dielectrics. Researchers said that high oxidative nature minimizes the charge density with a better heat transfer rate than kerosene dielectric [37]. Figure 12 indicates a surface roughness profile of AISI 316 under a kerosene dielectric medium. Hence, it is suggested to engage kerosene oil instead of transformer and canola oils when EDM of AISI 316 material is anticipated.

Alike MRR, the effect of different electrodes is also studied on TWR, as portrayed in Fig. 11. The literature said that TWR is inversely proportional to the melting temperature of the material [52]. For example, high melting temperature materials possess less TWR or vice versa. Considering this concept, it has been found that the melting temperature of copper (1085 °C) is higher, followed by brass (927 °C) and aluminium (660.3 °C) which translated into less wear and tore on the periphery of the copper electrode or resulting in less wide and deep craters such as presented in Fig. 13a. Thus, TWR is significantly decreased when the copper electrode is engaged for machining. In the case of an aluminium electrode, the value of TWR is also lessened than brass tool material owing to its higher thermal conductivity (227.0 W/mK) compared to brass (109.0 W/mK). High thermal conductivity allows a quicker heat transfer rate through the aluminum than brass during each spark, decreasing the TWR

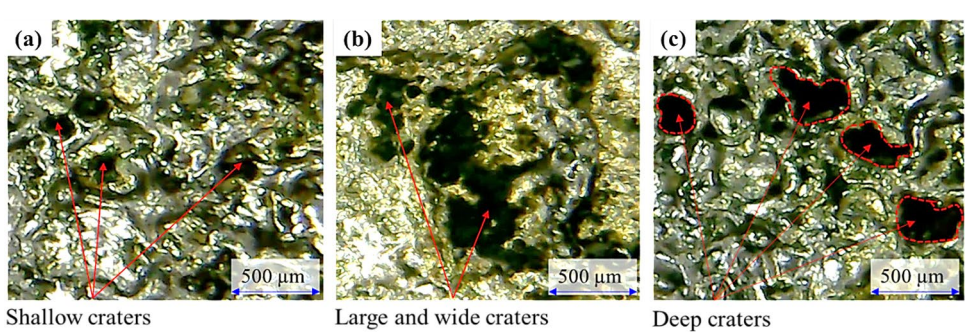

Fig. 13 Effect of different electrodes on the formation of craters' size: **a** copper, **b** brass, and **c** aluminum

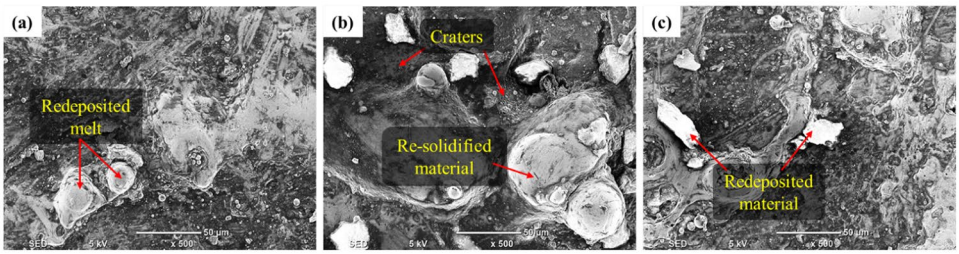

Fig. 14 SEM images (at 50 μm) illustrate melt re-deposition and craters on the AISI 316 for **a** copper, **b** brass, and **c** aluminum

by producing less wide but deep craters on the machined surface, as represented in Fig. 13c. Moreover, TWR is considerably elevated when the brass electrode is engaged for the machining of AISI 316 due to its low thermal conductivity compared to the rest of the electrodes. At low thermal conductivity, heat conduction through the metal body is hindered. Thus heat is largely retained at the tool interface, which translates into high TWR by leaving large and deep size craters, as portrayed in Fig. 13b [22].

SEM images, represented in Fig. 14, also show the craters and re-deposited material in the case of each electrode. The surface texture provided by the brass electrode is somewhat coarser than aluminium and copper. The rationale relies on the thermal conductivity of the electrodes. Since brass comprises lower thermal conductivity (109 W/mK) as compared to aluminium (205 W/mK) and copper (247 W/mK), deep craters are witnessed. As mentioned earlier, due to the low conductivity of the electrode, heat remains in the interface of the tool, which may lead to high TWR. Since the machined cavity is a replica of electrode surface quality, large and deep craters are achieved with brass because the said electrode comprises craters. A similar justification has been illustrated by Ahmed et al. [28]. Literature also revealed that thermal conductivity influences the formation of a recast layer on the machined surface [53]. Hence, to attain a minimum value of TWR, the copper electrode is the optimum for cutting AISI 316 via EDM.

The influence of various powders on the TWR is also presented in Fig. 11. A very slight deviation is noticed in the trend of electrode wear when powders are changed from alumina to SiC in the dielectric medium. However, the value of TWR upsurges to a maximum when SiC powder is utilized in the dielectric fluid because of its comparable melting temperature to alumina and graphite powder. This effect corresponds to the intensive ionization of the SiC particles in the machined gap. Then, these ionized particles hit the electrode surface with greater intensity and momentum. Hence, more wearing of the electrode takes place under SiC mixed dielectric. Moreover, concerning TWR, alumina powder is outperformed under the action of the EDM process. However, results with graphite powder are also nearly equal to the alumina powder as far as TWR is measured while machining AISI 316 through EDM. Since both powders generate spontaneous and uniform discharging, eliminating abnormal sparking, the wear rate of the electrode is improved [54].

The variation in the trend of TWR for the change in PTR (from 0.5 to 1.5) is demonstrated in Fig. 11. Initially, the trend declined up to PTR 1.0 and slightly deviated above up to PTR 1.5. The sharp decrease in the value of TWR from PTR 0.5 to 1.0 is due to the expansion of the plasma channel, which hinders the effective heat input to the electrode and workpiece. Since the electrode experiences insufficient heat energy, its wear rate is notably decreased [22]. However, with the further change in the pulse-time ratio to 1.5, the TWR reasonably increased. It is credited to the reason high PTR implies that discharge energy insists on a longer duration. This generates enormous heat energy in the cutting zone, increasing material melting from both the workpiece and tool [22]. Consequently, TWR is increased. Figure 15 depicts the surface textures formed at three levels of PTR. It is worth observing that different sizes of craters are recognized at different pulse time ratios. For example,

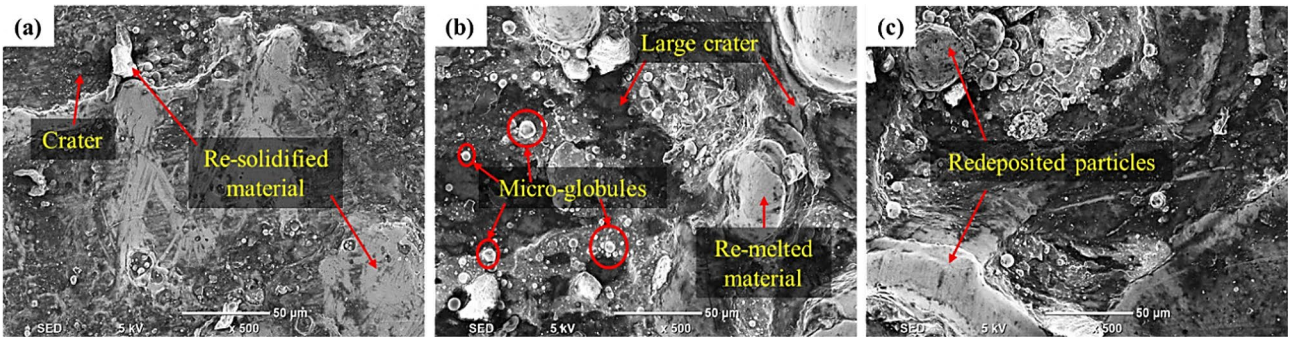

Fig. 15 Surface's condition on AISI 316 at different settings of PTR: **a** 0.5, **b** 1.0, and **c** 1.5

at lower PTR, the surface of the machined cavity contains shallow and small size craters, whereas, in the rest of the cases, large and deep craters were found on the surface of the workpiece, as witnessed in Fig. 15. The large size craters noticed in the latter case are due to the generation of extensive heat energy in the plasma gap caused by the prolonged machining/sparking time with respect to pulse off-time. The opposite reason is true for other situations. Moreover, at the higher magnitude of PTR, more material gets re-deposited over the substrate's surface even micro-globules are formed. The formation of micro-globules on the machined profile is due to partially evaporated material in lieu of condensed material. Researchers claimed that re-deposited material has no significant effect on the surface integrity of the substrate material, while the micro-globules may provide a site to grow stress concentration [55]. Thus, the strength of the material can be affected. Hence, the second level of PTR (1.0) is best suited for achieving the minimum TWR considering the EDM of AISI 316 material.

Alike MRR, the interaction plot of TWR is also discussed herein, as represented in Fig. 16. Between the two factors, i.e., dielectric type and electrode type, all the dielectrics intersect when the copper electrode is engaged during the cutting of AISI 316. At the same time, no relationship is identified against the brass electrode. Two dielectrics (transformer and canola oil) have shown the interactive effect for the aluminum tool, while kerosene oil remains safe from any influence. Considering the interaction effect between powder type and dielectric type, it can be reported that all the dielectrics have interactions with the different powders. The same behavior is also predicted in the interaction plot made between PTR and dielectric type. It is pertinent to mention that aluminum is the only electrode that provided a relationship with the copper tool at the third level of powder type and PTR, as far as interaction plots between electrode type-powder type and electrode type-PTR are considered, respectively. Such effects can be observed in the interaction plots presented in Fig. 16. To evaluate TWR for the previously said interaction plots, level 1 of each against the copper electrode is an optimal case. Finally, for the last interaction plot between PTR and powder type, each powder has a relationship at all levels of PTR.

3.3 Overcut versus input parameters

The main purpose of advanced technologies is to develop components with high geometric accuracy and precision. For that rationale, they require a detailed study of overcut so that the intended functionality of products can be ensured. Thereof, in this investigation, the dimensional accuracy in terms of overcut (OC) is also considered against the set of control parameters during EDM of AISI 316. The main effect plots in Fig. 17 illustrate the influence of each parameter on the diametrical OC.

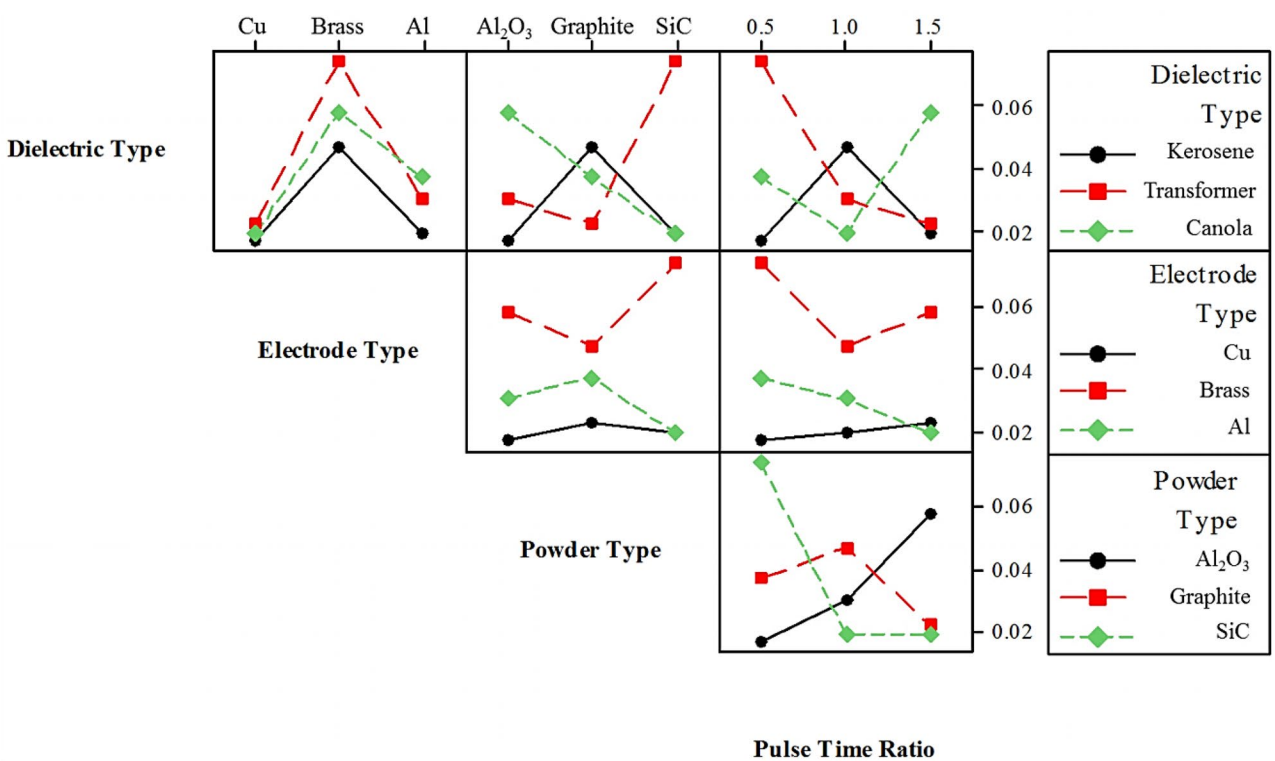

Fig. 16 Interaction plot (data mean) of tool wear rate

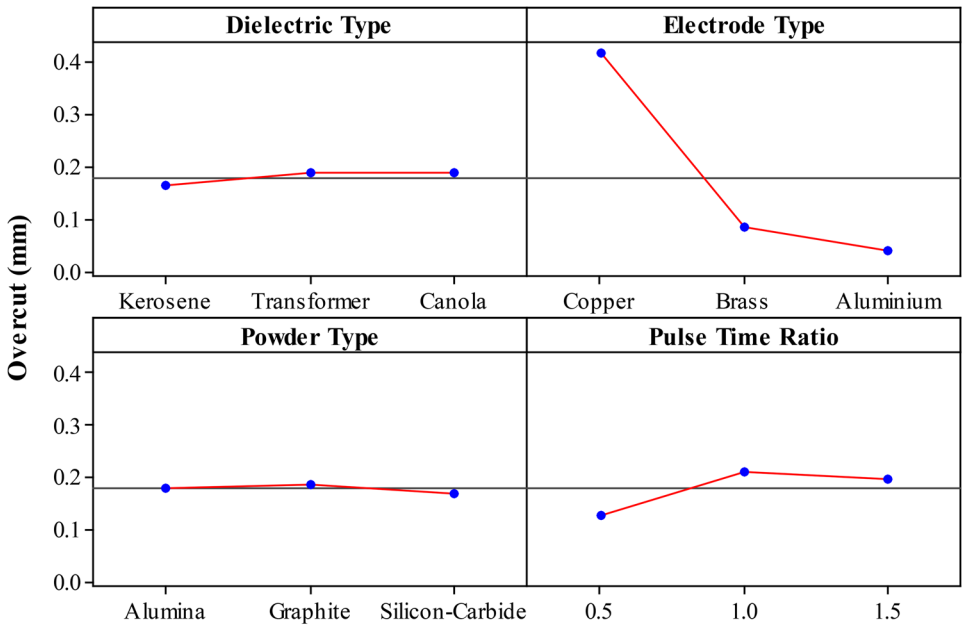

Fig. 17 Main effect plot of overcut versus different parameters

As stated earlier, three different oils (kerosene, transformer, and canola) have been used as dielectric fluid to machine AISI 316 by utilizing the EDM technique. Likewise, other responses, the effects of elected dielectrics are evaluated about diametrical OC, as shown in Fig. 17. It has been inferred from Fig. 17 that a minimum OC value was achieved with kerosene oil. The reason is linked to the fewer flash point of kerosene oil (38 °C) followed by transformer oil (140 °C) and canola oil (330–360 °C). Due to low flash points, kerosene oil yielded fewer ionized particles than the rest of the dielectrics. Thus, the spark is more stabilized or less diverged, which improves the OC [56]. Interestingly, transformer and canola oil yielded the same magnitude of OC. Still, they both are unsuitable for geometrical accuracy when comparison has been made with kerosene dielectric. Thereof, kerosene dielectric can be preferred over the rest of the dielectrics to attain minimal diametrical OC as long as EDM of AISI 316 is discussed. The SEM images represented in Fig. 18 illustrate the surface morphology achieved under each dielectric type. According to Fig. 18, shallow craters are depicted on the surfaces obtained under selected dielectrics. However, the surface texture attained with transformer oil is coarsest than the canola and kerosene oils. The high non-biodegradability of transformer oil could be the key reason behind this. Also, the mentioned oil belongs to the class of hydrocarbons, which produce carbon particles during the discharge process. These particles may cause hindrance in front of sparking, and thus, the probability of material re-deposition is enhanced. For that reason, extensive re-deposition of melted particles can also be noticed on the surface morphology, as represented in Fig. 18b.

The effect of different tools on the OC is also presented in Fig. 17. A decreasing trend is attained from copper to aluminum electrodes. It means aluminium electrode has performed outstandingly in terms of OC, followed by brass and copper electrodes when AISI 316 is used for machining on EDM. Less thermal conductivity is the main motive behind the excellent performance of the aluminum electrode. The effect of low thermal conductivity causes less wear on the machined cavity due to insufficient spark energy. Thereof, better dimensional control is recorded with aluminum tool, and shallow craters are found on the work part surface, as shown in Fig. 19a. Furthermore, it can be seen that the diametrical overcut is more significant when the copper

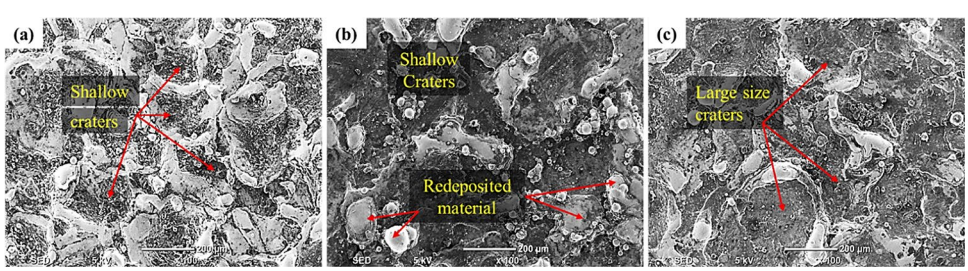

Fig. 18 Surface features obtained under various dielectrics: **a** kerosene oil, **b** transformer oil, and **c** canola oil

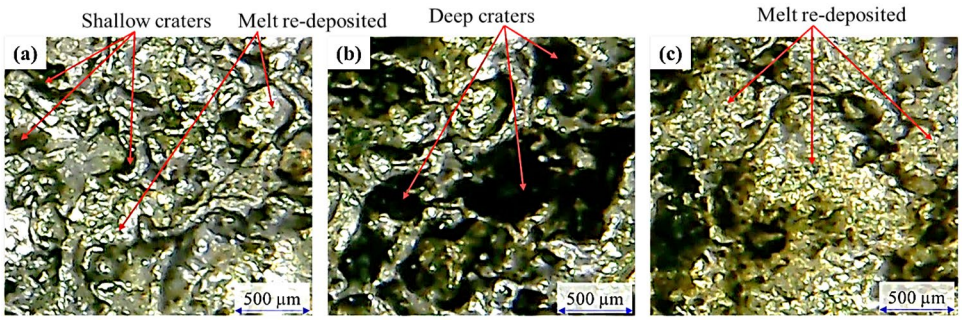

Fig. 19 Micrographs illustrate craters' size and re-deposited melt on the cut profile of AISI 316 against electrodes: **a** aluminum, **b** copper, and **c** brass

electrode is engaged. The reason lies precisely opposite to the case mentioned above for aluminium electrode. Such high thermal conductivity is the primary reason to obtain poor dimensional accuracy in the case of Cu-electrode. Due to heat conduction through the electrode, ionization of dielectric particles upsurges by applying high discharge energy in the cutting regime, resulting in more severe melting and vaporization of the material from the workpiece. As a result, dimensional accuracy is dropped with the copper electrode. However, deep craters are seen on the surface of the workpiece, as portrayed in Fig. 19b. Whereas brass has portrayed an intermediate response such that neither it is good like aluminum nor bad than copper owing to its magnetic nature as witnessed by Ishfaq et al. in their investigation [57]. The particles are re-deposited again on the material, as represented in Fig. 19c, and thus, the reasonable value of overcut is attained with the brass electrode. Hence, aluminum is the ideal electrode for achieving minimum OC. A graphical comparison of designated electrodes has also been developed using the minimum, average, and maximum magnitudes of OC, as demonstrated in Fig. 20.

Another trend of various powders on the OC is depicted in Fig. 17. A slight deviation from level 1 to level 3 of powder type is noticed. It has been further noted that powder type has minimal effect on the diametral OC compared to the other parameters. However, less magnitude of OC value is obtained when SiC is mixed in the dielectric fluid during EDM of AISI 316. It is attributed to the thermo-physical nature of SiC powder and its excellent electrical resistivity among the selected powders. Moreover, the high density of SiC powder resists the homogeneity in the dielectric medium. These two reasons lead to low OC [58]. Contrary to that, the magnitude of OC is raised when graphite powder is added to the dielectric liquid due to its high conductive nature than SiC and Al_2O_3 powders. As per the published work, the addition of conductive powders in the dielectric enlarged the machining gap and dispersed the plasma channel by minimizing the breakdown strength of the dielectric. Because of low breakdown strength, sparking is occurred from a longer distance, resulting in an increment of OC [58]. It is further seen that alumina powder has also shown the same outcomes as depicted for graphite powder. The surface texture obtained under each powder type is provided in Fig. 21. The imperfections like craters, voids, and resolidified materials are found in every case shown in Fig. 21. The craters formed under all the powders during EDM of AISI 316 are shallow and large. Additionally, depending upon the behavior of every powder in the dielectric regime, different volumes of materials are resolidified on the substrate's cavity. However, the SiC powder is superior to other powders, and therefore, it is suggested to use it in the dielectric liquid to attain a good dimensional accuracy.

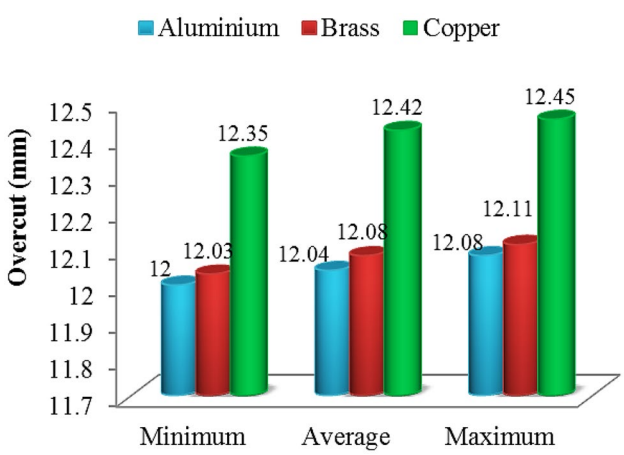

Fig. 20 Comparison of minimum, average, and maximum OC versus electrode materials

The impact of PTR on the OC is also shown in Fig. 17. Initially, the trend shifted up by the varying value of PTR from 0.5 to 1.0 and then slightly declined up to PTR 1.5. The increment in the value of OC between PTR 0.5–1.0 is due to a greater flow of current per cycle that causes extensive ionization of the dielectric particles between the workpiece and electrode space. This excessive ionization caused the dissolution of ions over the machined cavity, leaving behind large craters as shown in Fig. 22a, and thereof correspondingly value of OC is magnified in the said range of PTR [59]. It can be perceived from Fig. 17 that with the further increase of PTR to 1.5, the OC is again improved, which is because of

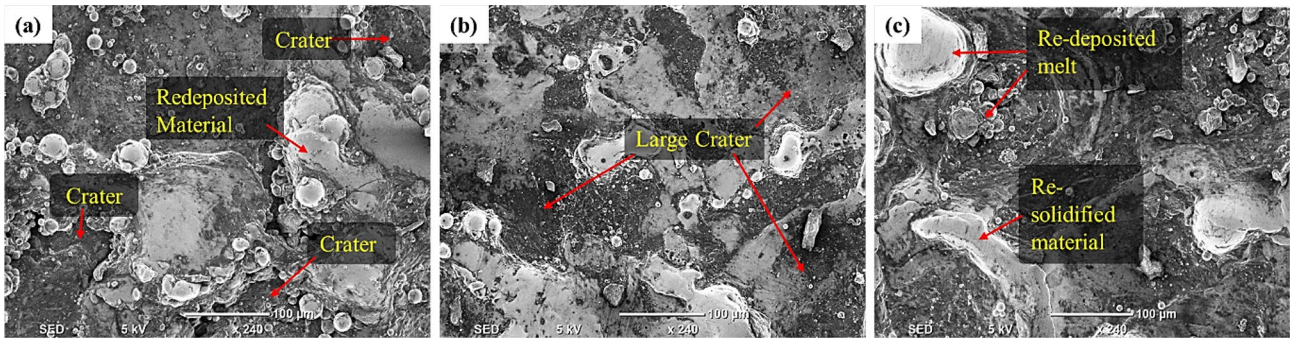

Fig. 21 Surface texture attained under different powders: **a** alumina, **b** graphite, and **c** silicon carbide

liberating more heat energy at highly high T_{on} (75 µs). This heat energy makes a pool of ions, re-melted material, and some dielectric particles above the cutting surface, which act as a shield/cover of protection for sparking. As a result, less material is chipped out from the workpiece, decreasing the OC [57]. At this condition, shallow craters are noticed on the machined cavity of the work part, as depicted in Fig. 22b. Thus, level 1 (0.5) of PTR is highly favorable for getting minimum diametral OC when EDM of selected biomedical material is deliberated.

Figure 23 depicts the interaction plots of overcut. According to Fig. 23, the two input parameters, i.e., dielectric type and electrode type, have more excellent interactions. Similarly, for the interaction plot between dielectric type versus powder type and dielectric type versus PTR, trends for all the dielectrics intersect each other at different points against the parametric levels of both powder type and PTR. It means significant interactions exist there. However, for the interaction plot between powder type and electrode type, no relationship(s) is found with the copper electrode (providing poor geometric accuracy or high OC), although the trends of other electrodes intersect at two places concerning the second factor. Similar effects are detected in the interaction plot between PTR and electrode type, as indicated in Fig. 23. In the last interaction plot between powder type and PTR, alumina, graphite, and SiC powders have different interactions with each other for the values of PTR.

Taking the effect of all input factors collectively, the optimal setting for attaining the maximum MRR, minimum TWR, and OC while EDM of AISI 316 is tabulated in Table 4. Such as the optimal combination for getting high MRR using Cu electrode is dielectric type = transformer oil, powder type = SiC, and PTR = 1.0. The same parametric setting is also noticed with TWR, but alumina and kerosene oil have been proved to be the best ones instead of SiC powder and transformer oil, respectively. Similarly, high dimensional accuracy on the surface of AISI 316 has been

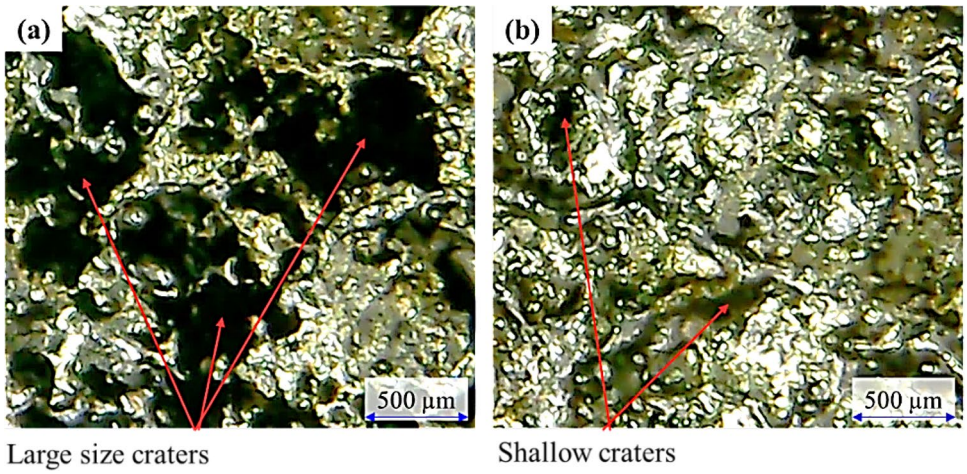

Fig. 22 Influence of PTR on the size of craters when **a** PTR = 1.0 and **b** PTR = 1.5

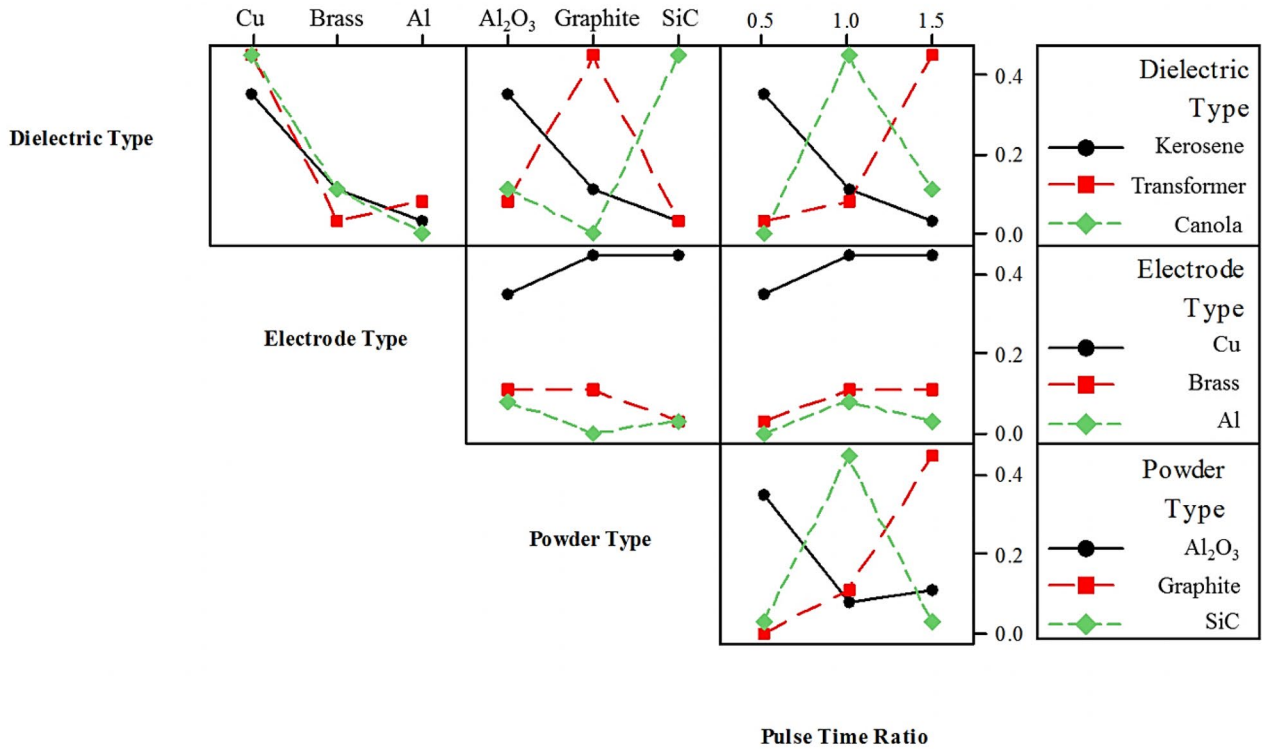

Fig. 23 Interaction plot (data mean) of overcut

achieved under SiC mixed kerosene dielectric when the Al-electrode is utilized with PTR equal to 0.5. The combinations provided in Table 4 have also been confirmed through confirmation trials.

3.4 Multiobjective optimization strategy

It is pertinent to mention that MRR, TWR, and OC have variations in magnitude, and the effect of some of the input variables is unlike them. For that reason, a multiobjective optimization strategy, such as GRA, was employed to find an optimal parametric setting. The findings of GRA are summarized in Table 5. According to the results of GRA, the preferred alternative that can improve the responses mentioned above is alternate no. 3. The proposed optimized setting, tabulated in Table 6, was further tested through a confirmation run.

The findings of the confirmation run are compiled in Table 7. It can be noticed that the responses' magnitude is significantly improved when cutting of AISI 316 through the EDM process is under consideration by using the optimal setting presented in Table 6. According to Table 7, 29% and 89.4% improvements from the average response value have been found in the magnitude of MRR and TWR, respectively.

Table 4 Optimal parametric setting against each output parameter

Responses' name	Material removal rate	Tool wear rate	Overcut
Optimal settings	Dielectric type: transformer oil Electrode type: Cu Powder type: SiC PTR: 1.0	Dielectric type: kerosene oil Electrode type: Cu Powder type: Al_2O_3 PTR: 1.0	Dielectric type: kerosene oil Electrode type: Al Powder type: SiC PTR: 0.5

Table 5 GRA-based alternates' ranking

Exp. no.	Gray relational generation			Gray relational coefficients			GRA grades calculation and alternates' ranking	
	MRR	TWR	OC	MRR (GC)	TWR (GC)	OC (GC)	GRA grades	GRA ranking
Xo	1	1	1					
1	0.31	1.00	0.24	0.42	1.00	0.40	0.61	5
2	0.00	0.47	0.81	0.33	0.49	0.72	0.51	8
3	0.69	0.96	1.00	0.61	0.93	1.00	0.85	1
4	1.00	0.91	0.00	1.00	0.85	0.33	0.73	3
5	0.11	0.00	1.00	0.36	0.33	1.00	0.56	7
6	0.98	0.77	0.88	0.96	0.69	0.81	0.82	2
7	0.79	0.96	0.00	0.70	0.93	0.33	0.66	4
8	0.08	0.28	0.81	0.35	0.41	0.72	0.50	9
9	0.04	0.65	0.86	0.34	0.59	0.78	0.57	6

Table 6 A single optimized parametric setting

Parameters	Optimal setting
Dielectric type	Kerosene oil
Electrode type	Aluminium
Powder type	Silicon carbide
Pulse time ratio	1.5

Table 7 Confirmation trial results

Optimal settings	Responses' magnitude		
	MRR (g/min)	TWR (g/min)	OC (mm)
Dielectric type: kerosene oil Electrode type: aluminium Powder type: silicon carbide Pulse time ratio: 1.5	0.111	0.019	0.03
Average values of responses observed during whole experimentation	0.086	0.036	0.189
Improvement in response parameters	29%	89.4%	5.3 times

Moreover, the magnitude of OC is 5.3 times less than its average value. After a noteworthy improvement in various output parameters, it can be concluded that the proposed optimized setting is the best combination to enhance the machining rate and reduce geometrical errors during EDM of AISI 316.

4 Conclusions

The current article studied material removal rate, tool wear rate, and overcut for the EDM of AISI 316 material. The effect of said responses was treated comprehensively against the defined input parameters. For experimentation, Taguchi L9 orthogonal approach was applied to foresee the micro-impressions on the selected workpiece. Results were analyzed by main effect plots, whereas evidence was collected through SEM, optical microscope, and surface profilometry. The optimized parametric setting for each response has been suggested. A single optimal setting, that optimized the machine variables, was also made using grey relational analyses. The possible conclusions can be drawn from the experimental results.

- Among various dielectrics, kerosene dielectric is outperformed in terms of TWR and OC. However, transformer oil gives a better material removal rate than other dielectrics due to its high thermal oxidative nature.
- Regardless of different dielectrics, the copper tool erodes the workpiece appreciably and delivers minimum tool wear rate due to its high melting temperature, followed by brass and aluminium. Moreover, aluminium is the best alternative for attaining considerable geometric accuracy.

- For the third parameter, different powders were added to the dielectric fluid. According to the results, the SiC powder performs better in the context of MRR and OC. At the same time, alumina powder allows a reduction in the value of TWR, followed by other powders.
- In the case of pulse time ratio, level 2 (1.0) is a highly novel setting to get the maximum MRR and less TWR because of the expansion of the plasma channel, which hinders the effective heat input to the electrode and workpiece. Since the electrode experiences insufficient heat energy, thereof less wear rate of the electrode is observed at PTR 1.0. Contrarily, the lowest OC is observed at PTR 0.5.
- A single optimized setting proposed through the GRA approach improves the magnitude of all responses. In particular, from the mean values of responses, 29% and 89.4% improvement in the magnitude of MRR and TWR are noted, respectively. Furthermore, the value of diametrical overcut is 5.3 times reduced than its average magnitude. Hence, for the EDM of AISI 316, the optimal parametric combination to enhance machining efficiency and geometric accuracy is dielectric type: kerosene oil, electrode type: aluminium, powder type: silicon carbide, and pulse time ratio: 1.5.

Author contribution Authors have notable contributions for the preparation of this manuscript.

Funding Open Access funding provided by the Qatar National Library.

Data availability The data gathered for this study is presented.

Code availability Not applicable.

Declarations

Ethics approval Not applicable.

Consent to participate All authors agreed to participate in this work.

Consent for publication All authors are agreed for publication of this work.

Conflict of interest The authors declare no competing interests.

Open Access This article is licensed under a Creative Commons Attribution 4.0 International License, which permits use, sharing, adaptation, distribution and reproduction in any medium or format, as long as you give appropriate credit to the original author(s) and the source, provide a link to the Creative Commons licence, and indicate if changes were made. The images or other third party material in this article are included in the article's Creative Commons licence, unless indicated otherwise in a credit line to the material. If material is not included in the article's Creative Commons licence and your intended use is not permitted by statutory regulation or exceeds the permitted use, you will need to obtain permission directly from the copyright holder. To view a copy of this licence, visit http://creativecommons.org/licenses/by/4.0/.

References

1. Alting L, Kimura F, Hansen HN, Bissacco G (2003) Micro engineering. CIRP Ann 52:635–657. https://doi.org/10.1016/S0007-8506(07)60208-X
2. Rahman M, Asad ABMA, Masaki T, Saleh T, Wong YS, Senthil Kumar A (2010) A multiprocess machine tool for compound micromachining. Int J Mach Tools Manuf 50:344–356. https://doi.org/10.1016/j.ijmachtools.2009.10.007
3. Jahan MP, Rahman M, Wong YS (2014) Micro-electrical discharge machining (micro-EDM). In: Comprehensive Materials Processing. Elsevier, pp 333–371
4. Pramanik A, Basak AK, Littlefair G, Debnath S, Prakash C, Singh MA, Marla D, Singh RK (2020) Methods and variables in Electrical discharge machining of titanium alloy – A review. Heliyon 6:e05554. https://doi.org/10.1016/j.heliyon.2020.e05554
5. Oke SR, Ogunwande GS, Onifade M, Aikulola E, Adewale ED, Olawale OE, Ayodele BE, Mwema F, Obiko J, Bodunrin MO (2020) An overview of conventional and non-conventional techniques for machining of titanium alloys. Manuf Rev 7:34. https://doi.org/10.1051/mfreview/2020029
6. Manjaiah M, Narendranath S, Basavarajappa S (2014) Review on non-conventional machining of shape memory alloys. Trans Nonferrous Met Soc China 24:12–21. https://doi.org/10.1016/S1003-6326(14)63022-3
7. Shreyas RR, Sachin BKSK, Nanjundeswaraswamy TS (2019) Selection of non-traditional machining process. Int J Eng Res Technol 8:148–155
8. Snoeys R, Staelens F, Dekeyser W (1986) Current trends in non-conventional material removal processes. CIRP Ann 35:467–480. https://doi.org/10.1016/S0007-8506(07)60195-4
9. Kibria G, Sarkar BR, Pradhan BB, Bhattacharyya B (2010) Comparative study of different dielectrics for micro-EDM performance during microhole machining of Ti-6Al-4V alloy. Int J Adv Manuf Technol 48:557–570. https://doi.org/10.1007/s00170-009-2298-y
10. Shastri RK, Mohanty CP, Dash S, Gopal KMP, Annamalai AR, Jen C-P (2022) Reviewing performance measures of the die-sinking electrical discharge machining process: challenges and future scopes. Nanomaterials 12:384. https://doi.org/10.3390/nano12030384
11. John P, Davis R (2016) Performance study of electrical discharge machining process in burr removal of drilled holes in Al 7075. Cogent Eng 3:1270702. https://doi.org/10.1080/23311916.2016.1270702
12. Dehghani D, Yahya A, Khamis NH (2020) Dynamic behaviour of EDM system through mathematical model. J Phys Conf Ser 1529:052001. https://doi.org/10.1088/1742-6596/1529/5/052001
13. Abu Qudeiri J, Saleh A, Ziout A, Mourad A-H, Abidi M, Elkaseer A (2019) Advanced electric discharge machining of stainless steels: assessment of the state of the art, gaps and future prospect. Materials (Basel) 12:907. https://doi.org/10.3390/ma12060907
14. Ho K, Newman S (2003) State of the art electrical discharge machining (EDM). Int J Mach Tools Manuf 43:1287–1300. https://doi.org/10.1016/S0890-6955(03)00162-7
15. Wang J, Han F, Cheng G, Zhao F (2012) Debris and bubble movements during electrical discharge machining. Int J Mach Tools Manuf 58:11–18. https://doi.org/10.1016/j.ijmachtools.2012.02.004
16. Abulais S (2014) Current Research trends in electric discharge machining (EDM): review. Int J Sci Eng Res 5:100–118
17. Guu YH, Hocheng H (2013) Electrical discharge machining. In: Hocheng H, Tsai H-Y (eds) Advanced analysis of nontraditional machining. Springer, New York, New York, NY, USA, pp 65–106
18. Sharma P, Singh S, Mishra DR (2014) Electrical discharge machining of AISI 329 stainless steel using copper and brass

rotary tubular electrode. Procedia Mater Sci 5:1771–1780. https://doi.org/10.1016/j.mspro.2014.07.367
19. Kumar S, Ghoshal SK, Arora PK, Nagdeve L (2021) Multi-variable optimization in die-sinking EDM process of AISI420 stainless steel. Mater Manuf Process 36:572–582. https://doi.org/10.1080/10426914.2020.1843678
20. Abdulkaree S, Khan AA, Zain ZM (2011) Effect of machining parameters on surface roughness during wet and drywire-EDM of stainless steel. J Appl Sci 11:1867–1871. https://doi.org/10.3923/jas.2011.1867.1871
21. Prathipati R, Ch R, Dora SP (2019) Corrosion behavior of surface induced by wire EDM on 316L stainless steel: an experimental investigation. SN Appl Sci 1:952. https://doi.org/10.1007/s42452-019-0992-4
22. Ishfaq K, Asad M, Anwar S, Pruncu CI, Saleh M, Ahmad S (2020) A Comprehensive analysis of the effect of graphene-based dielectric for sustainable electric discharge machining of Ti-6Al-4V. Materials (Basel) 14:23. https://doi.org/10.3390/ma14010023
23. Muthuramalingam T, Mohan B (2015) A review on influence of electrical process parameters in EDM process. Arch Civ Mech Eng 15:87–94. https://doi.org/10.1016/j.acme.2014.02.009
24. Ramachandra R (2017) Optimization of MRR and SR for AISI 316 Stainless steel material by using RSM Technique in EDM machining. Int J Eng Sci Math 6:314–321
25. Majumder A (2013) Process parameter optimization during EDM of AISI 316 LN stainless steel by using fuzzy based multi-objective PSO. J Mech Sci Technol 27:2143–2151. https://doi.org/10.1007/s12206-013-0524-x
26. Makwana AV, Banker KS (2015) An experimental investigation on AISI 316 stainless steel for tool profile change in die sinking EDM using DOE. Sch J Eng Technol 3:447–462
27. Safiei W, Sharif S, Mansor AF, Mohd Isa MH (2014) Performance evaluation of electrical discharge machining die sinking on stainless steel 316L using copper impregnated graphite. Appl Mech Mater 660:48–54. https://doi.org/10.4028/www.scientific.net/AMM.660.48
28. Ahmed N, Anwar S, Ishfaq K, Rafaqat M, Saleh M, Ahmad S (2019) The potentiality of sinking EDM for micro-impressions on Ti-6Al-4V: keeping the geometrical errors (axial and radial) and other machining measures (tool erosion and work roughness) at minimum. Sci Rep 9:17218. https://doi.org/10.1038/s41598-019-52855-6
29. Ishfaq K, Farooq MU, Pruncu CI (2021) Reducing the geometrical machining errors incurred during die repair and maintenance through electric discharge machining (EDM). Int J Adv Manuf Technol 117:3153–3168. https://doi.org/10.1007/s00170-021-07846-1
30. Chen S, Lian M, Wu X, Lei J, Zhao H, Peng T, Luo F, Yang J, Xu B (2021) Study on the micro-EDM processing characteristics of Ti-6Al-4V alloy with different electrode materials. Int J Adv Manuf Technol 116:3369–3376. https://doi.org/10.1007/s00170-021-07664-5
31. Wang X, Yi S, Guo H, Li C, Ding S (2020) Erosion characteristics of electrical discharge machining using graphene powder in deionized water as dielectric. Int J Adv Manuf Technol 108:357–368. https://doi.org/10.1007/s00170-020-05405-8
32. Pour M, Javadi SM, Layegh E (2022) Influence of ZnO nanoparticle addition and spark peak current on EDM process of AISI 1045, AISI 4140, and AISI D3: MRR, surface roughness, and surface topography. Int J Adv Manuf Technol. https://doi.org/10.1007/s00170-022-10090-w
33. Tiwary AP, Pradhan BB, Bhattacharyya B (2018) Investigation on the effect of dielectrics during micro-electro-discharge machining of Ti-6Al-4V. Int J Adv Manuf Technol 95:861–874. https://doi.org/10.1007/s00170-017-1231-z
34. Raju P, Sarcar MMM, Satyanarayana B (2014) Optimization of wire electric discharge machining parameters for surface roughness on 316 L stainless steel using full factorial experimental design. Procedia Mater Sci 5:1670–1676. https://doi.org/10.1016/j.mspro.2014.07.355
35. Ostovan F, Shafiei E, Toozandehjani M, Mohamed IF, Soltani M (2021) On the role of molybdenum on the microstructural, mechanical and corrosion properties of the GTAW AISI 316 stainless steel welds. J Mater Res Technol 13:2115–2125. https://doi.org/10.1016/j.jmrt.2021.05.095
36. Kompelli G, Rasool Shaik KN, Manimaran HP, Injeti W (2019) Comparative studies of EDM machining using aluminium, brass, copper. Int J Eng Appl Sci Technol 04:243–254. https://doi.org/10.33564/IJEAST.2019.v04i08.043
37. Rao KM, Kumar DV, Shekar KC, Singaravel B (2020) Experimental analysis of canola oil as dielectric fluid in electric discharge machining of AISI D2 steel. Mater Sci Forum 978:49–54. https://doi.org/10.4028/www.scientific.net/MSF.978.49
38. Murugesh S, Manikandan N, Subramaniyan M, Chockalingam S, Surendar G (2021) Experimental investigation of electrode shape configuration in sustainable electric discharge machining process. IOP Conf Ser Mater Sci Eng 1057:012068. https://doi.org/10.1088/1757-899X/1057/1/012068
39. Kumar Sahu S, Dey B, Datta S (2019) Selection of appropriate powder-mixed dielectric media (kerosene and used transformer oil) for desired EDM performance on Inconel 718 super alloys. Mater Today Proc 18:4111–4119. https://doi.org/10.1016/j.matpr.2019.07.355
40. Rathi MG, Mane DV (2014) Study on effect of powder mixed dielectric in EDM of Inconel 718. Int J Sci Res Publ 4:1–7
41. Shabgard M, Rezaei Zaki M, Abbasi H (2019) Experimental investigation on the effect of SiC particles in machining process of Al–5.3% CU-SiCp–Al2O3p hybrid nanocomposite by EDM. SN Appl Sci 1:434. https://doi.org/10.1007/s42452-019-0401-z
42. Unses E, Cogun C (2015) Improvement of electric discharge machining (EDM) performance of Ti-6Al-4V alloy with added graphite powder to dielectric. Strojniški Vestn – J Mech Eng 61:409–418. https://doi.org/10.5545/sv-jme.2015.2460
43. Deepak B, Parhi D, Jena PC (2020) Innovative product design and intelligent manufacturing systems. Springer Singapore, Singapore
44. Mahajan R, Krishna H, Singh AK, Ghadai RK (2018) A review on copper and its alloys used as electrode in EDM. IOP Conf Ser Mater Sci Eng 377:012183. https://doi.org/10.1088/1757-899X/377/1/012183
45. Gudur VV, Potdar S (2015) Effect of silicon carbide powder mixed EDM on machining characteristics of SS 316L material. Int J Innov Res Sci Eng Technol 04:2003–2007. https://doi.org/10.15680/IJIRSET.2015.0404027
46. Sharma R, Singh J (2014) Effect of powder mixed electrical discharge machining (PMEDM) on difficult-to-machine materials – a systematic literature review. J Manuf Sci Prod 14:233–255. https://doi.org/10.1515/jmsp-2014-0016
47. Kolli M, Kumar A (2015) Effect of dielectric fluid with surfactant and graphite powder on Electrical Discharge Machining of titanium alloy using Taguchi method. Eng Sci Technol an Int J 18:524–535. https://doi.org/10.1016/j.jestch.2015.03.009
48. Gattu SD, Yan J (2022) Micro Electrical discharge machining of ultrafine particle type tungsten carbide using dielectrics mixed with various powders. Micromachines 13:998. https://doi.org/10.3390/mi13070998
49. Yeo SH, Tan PC, Kurnia W (2007) Effects of powder additives suspended in dielectric on crater characteristics for micro electrical discharge machining. J Micromech Microeng 17:N91–N98. https://doi.org/10.1088/0960-1317/17/11/N01

50. Kibria G, Bhattacharyya B (2017) Microelectrical discharge machining of Ti-6Al-4V. In: Microfabrication and Precision Engineering. Elsevier, pp 99–142
51. Rao KM, Kumar DV, Singaravel B, Pradesh A (2020) State of the art in green dielectric fluid for sustainable electrical discharge. J Crit Rev 7:6192–6204. https://doi.org/10.31838/jcr.07.19.716
52. Bhaumik M, Maity K (2018) Effect of different tool materials during EDM performance of titanium grade 6 alloy. Eng Sci Technol an Int J 21:507–516. https://doi.org/10.1016/j.jestch.2018.04.018
53. Khan AA (2008) Electrode wear and material removal rate during EDM of aluminum and mild steel using copper and brass electrodes. Int J Adv Manuf Technol 39:482–487. https://doi.org/10.1007/s00170-007-1241-3
54. Alam ST, Amin AN, Hossain MI, Huq M, Tamim SH (2021) Performance evaluation of graphite and titanium oxide powder mixed dielectric for electric discharge machining of Ti–6Al–4V. SN Appl Sci 3:435. https://doi.org/10.1007/s42452-021-04450-6
55. Arooj S, Shah M, Sadiq S, Jaffery SHI, Khushnood S (2014) Effect of current in the EDM machining of aluminum 6061 T6 and its effect on the surface morphology. Arab J Sci Eng 39:4187–4199. https://doi.org/10.1007/s13369-014-1020-z
56. Teimouri R, Baseri H (2012) Study of tool wear and overcut in EDM process with rotary tool and magnetic field. Adv Tribol 2012:1–8. https://doi.org/10.1155/2012/895918
57. Ishfaq K, Asad M, Harris M, Alfaify A, Anwar S, Lamberti L, Scutaru ML (2022) EDM of Ti-6Al-4V under nano-graphene mixed dielectric: a detailed investigation on axial and radial dimensional overcuts. Nanomaterials 12:432. https://doi.org/10.3390/nano12030432
58. Talla G, Gangopadhyay S, Biswas CK (2016) Effect of powder-suspended dielectric on the EDM characteristics of Inconel 625. J Mater Eng Perform 25:704–717. https://doi.org/10.1007/s11665-015-1835-0
59. Thanigaivelan R, Arunachalam RM (2010) Experimental study of overcut in electrochemical micromachining for 304 stainless steel. Trans North Am Manuf Res Inst SME 38:253–260

Publisher's Note Springer Nature remains neutral with regard to jurisdictional claims in published maps and institutional affiliations.